

Inelastic processes from vibrationally excited states in slow $H^+ + H_2$ and $H + H_2^+$ collisions: Excitations and charge transfer

Predrag S. Krstić

Physics Division, Oak Ridge National Laboratory, Oak Ridge, Tennessee 37831-6372

(Received 5 April 2002; revised manuscript received 18 July 2002; published 24 October 2002)

A comprehensive study is presented of the scattering of protons on $H_2(\nu_i)$ and of hydrogen atoms on $H_2^+(\nu_i)$, where ν_i is any vibrationally excited state of the relevant molecules. Cross sections for charge transfer and excitation have been calculated in the range of center-of-mass energies 0.6–9.5 eV using a fully quantal, coupled-channel approach. An extensive vibrational basis set, defined in a large configuration space of the reactants, is used, including a large number of discretized vibrational continua. A detailed picture is produced of all inelastic processes that involve two lowest, nonadiabatically coupled electronic surfaces of the H_3^+ molecule. The rotational dynamics of H_2 and H_2^+ are treated within the sudden approximation. The cross sections obtained are compared with the sparse data available from literature.

DOI: 10.1103/PhysRevA.66.042717

PACS number(s): 34.70.+e, 82.30.Fi

I. INTRODUCTION

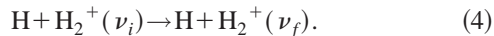
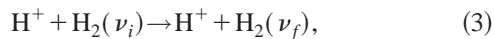
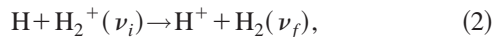
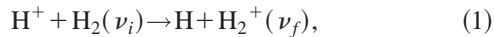
The proton-hydrogen molecule and hydrogen-hydrogen-molecular-ion systems (which is referred to simplify as the H_3^+ collision system) are the most fundamental ion-atom and ion-molecule two-electron collision systems. A typical collision event evolves through dynamically coupled electronic, vibrational and rotational degrees of freedom. These systems have been studied thoroughly only for the processes from the ground states (electronic, vibrational, rotational) as motivated by applications, as well as limited by experimental and theoretical capabilities of the time. The majority of the theoretical treatments in eV and ten-eV ranges of collision energies have been carried out for $H^+ + H_2$ within the infinite order sudden approximation (IOSA) for rotations, implying that the collision center-of-mass (c.m.) energy, $E_{c.m.}$, is well above the value of a typical quantum of rotational excitation of the H_2 target. Also, these calculations were done within a manifold of bound vibrational states, thus neglecting the possible importance of inelastic processes through “closed” dissociative channels, as well as the dynamic change of the dissociative continuum edge with the position of the projectile. Therefore, there is, even with IOSA, a fundamental interest in obtaining the cross sections for transitions between bound vibrational states (charge transfer, excitation) from both ground and excited vibrational states of the target molecule (H_2 or H_2^+). This interest has been recently elevated by need for the charge transfer (CT) data from excited states of H_2 to a proton projectile in a relatively cold (~ 1 – 10 eV) divertor plasma of a fusion tokamak [1–5]. The cold divertor plasma regions are characterized by high neutral particle densities, with the presence of both H_2 and H_2^+ molecules. The CT process of hydrogen ions with vibrationally excited hydrogen molecules plays the dominant role in a chain of reactions that probably give the main contribution to the so called molecule assisted recombination (MAR). This process results in enhanced volumetric plasma recombination and promotion of the detached plasma regime. These regimes are necessary for the reduction of heat loads on divertor plates, one of the most serious problems in

today’s fusion energy research. An accurate knowledge of the cross sections (and/or of rate coefficients) for charge transfer for the entire spectrum of vibrationally excited molecules is of critical importance for evaluation of the role of MAR effects in a divertor plasma. An interest in CT between $H_2^+(\nu)$ and H has also recently arisen in astrophysics, in studies of evolution of the early universe, as one of the basic reactions in formation of the first neutral molecules. In the absence of dust grains, H_2 could only be formed through the gas-phase sequence of radiative processes followed by the CT reaction of H_2^+ and H [6].

The $H^+ + H_2(\nu_i)$ charge transfer reaction for $\nu_i \leq 3$, although endoergic, has a low threshold energy (1.83 eV for $\nu_i = 0$), and is strongly coupled to the mechanism of vibrational excitation to states that are high enough ($\nu \geq 4$) to overcome the barrier. Thus, this reaction is a second-order process for $\nu_i < 4$, with an integral cross section that is more than ten times lower than the cross section for excitation to the first excited state of H_2 for collision energies less than 200 eV [7]. On the other hand, charge transfer processes from higher excited states of H_2 are exoergic, often reflecting resonant features, with a significant role of nuclear particle exchange at eV energies, and may dominate inelastic transitions. Thus, the previously studied CT processes from lower ν_i constitute a separate group of processes (evolving through different physical mechanisms) from those for $\nu_i \geq 4$. Concerning the differential cross sections, in order for the electron to make a transition to the excited surface ($H + H_2^+$) the H_2 bond must stretch while the projectile is still close enough to the H_2 molecule. This indicates that CT processes inherently lead to large angle scattering. Similarly, collisions that involve nuclear rearrangements will almost always result in scattering to large angles. On the other hand the charge transfer process from H to H_2^+ is exoergic, i.e., there is no low-energy threshold, even from the ground $\nu_i = 0$ state of the target molecule.

The purpose of the present article is to calculate on the “same footing,” the cross sections for all inelastic processes in scattering of protons on $H_2(\nu_i \geq 0-14)$, as well as of scattering of hydrogen atoms on $H_2^+(\nu_i \geq 0-18)$. Specifically,

studied collisions are of the type



The text is organized in the following manner. Previous approaches to the problems (1)–(4) are reviewed in Sec. II, while details of the theory used are presented in Sec. III. Numerical procedures utilized are illustrated in Sec. IV, while results for charge transfer and excitation processes, Eqs. (1)–(4), are presented in Sec. V. In particular, the integral cross sections are shown and compared for the initial and final state resolved transitions in reacting $\text{H}^+ + \text{H}_2$ and $\text{H} + \text{H}_2^+$ systems. Conclusions are given in Sec. VI.

Atomic units are used throughout the text, unless otherwise explicitly stated.

II. PREVIOUS WORK

The comprehensive set of data for charge transfer for the collision system $\text{H}^+ + \text{H}_2(\nu)$ [8] in the energy range from threshold to several tens eV's, was recently calculated using the trajectory surface hopping (TSH) [9] method. The dynamics of the collision system (rotation, vibration, and motion of the projectile) were treated classically, while quantum transitions in isolated nonadiabatic regions are included by the two-state Landau-Zener model. Although the method incorporates rotational degrees of freedom into collision dynamics, thus going beyond the IOSA with respect to diatomic rotations, it has significant drawbacks: Besides the possible problems of a classical model for collision energies in the eV range and for treatment of lower vibrational and rotational states, the two-state nature of the transitions in the TSH may be oversimplifying the nature of electronic transitions in the system. A number of quantal cross-section calculations are also available for the $\text{H}^+ + \text{H}_2$ collision system, but only for processes from the ground vibrational state [10–18]. A detailed quantal study of elastic scattering of protons on H_2 in lower excited vibrational states, as well as vibrational excitation processes among these states, neglecting CT, have been reported recently [19–21]. Although the calculation of Top and Baer [22–24] for $\text{H}^+ + \text{H}_2$ in a collinear configuration was undertaken to include all inelastic vibrational processes in a narrow range of collision energies above the threshold for charge transfer, no results for cross sections could be reported. In fact, none of the studies mentioned have treated the H_3^+ collision system in a comprehensive and consistent manner, including all relevant inelastic processes with initially excited target molecules.

Approximations that can make a computation tractable depend on the properties of the collisional system, as well as on the process being considered and on the collision energy range. For example, in the range above a few hundred eV, the projectile is so fast that both the internuclear diatomic coordinate and its direction in space may be considered as frozen

during the collision. This significantly simplifies treatment of the collision dynamics of the electronic transitions, resulting in methods similar to those employed to treat ion-atom or atom-atom collisions. In contrast, consideration of the collision energies below 100 eV, down to about 1 eV, requires simultaneous coupling of the electronic and vibrational motions. In particular, the excitation energy of the first vibrational state of H_2 is ~ 0.5 eV corresponding to a characteristic vibration time exceeding 50 a.u., which is comparable to the collision time (of the order of $[\mu/2E]^{1/2}$) for energies ≤ 100 eV. The collision time is still short compared to the time scale of molecular rotations (excitation energy < 0.01 eV, i.e., the characteristic times > 1000 a.u.), thus enabling one to consider the direction of the diatomic internuclear axis as fixed. The consequence is that the angle, γ , defined as the angle between \vec{R} (defined from the center of mass of the molecule to the projectile nucleus) and diatomic internuclear axis $\vec{\rho}$, stays constant during a collision, i.e., enters the theory as a parameter. In effect, the equations of motion are completely decoupled as far as the angular variables are concerned. Conditions necessary for application of IOSA and interpretations of its parameters are widely discussed in the literature [25–34], within so-called energy sudden and centrifugal sudden approximations. It is generally accepted that IOSA is valid when the collision times are short on the scale of rotational periods of the molecule, such that ion-molecule orientation stays nearly fixed during the interaction time of the collision. It works the best for small values of the projectile orbital momentum and if the molecule is in low rotational state [15,26].

In addition, the high degree of symmetry in the H_3^+ system, studied here, results in potential surfaces that are to the high degree isotropic (independent of γ) [11]. Since, in the limit of an isotropic potential both orbital and molecule angular momenta become decoupled, the IOSA is expected to work well from a fraction of an eV collision energy and above. Still, to include the effects of anisotropy of the electronic potential with respect to γ , especially at small internuclear distances, one needs to calculate the observables for different values of γ and then average over them. It is consistent with IOSA to neglect electronic-nuclear rotational coupling [34].

Due to the simplicity of the hydrogen atom the processes listed, Eqs. (1)–(4), are among the simplest of all ion- or atom-molecule collisions. The reduction of the problem to the coupling of only electronic and vibrational states simplifies the three-atomic collision problem enormously. Still, a comprehensive *ab initio* numerical treatment of the problem, even within IOSA, is a formidable, difficult computational task, especially when accounting for the presence of reactions with interchange of nuclear particles. In principle, this requires simultaneous treatment of several configuration spaces with different nuclear arrangements, which causes a multiple increase in the dimensionality of the problem. Various approximations have been proposed to overcome this problem, the most often used is reactive IOSA (RIOSA) [31–33,35–37], where coupling between various nuclear ar-

rangements is done after performing calculations in each configuration space independently. The boundary conditions for the problem are propagated into different arrangements by matching the wave functions along the assumed borders between nuclear configurations. Due to the complicated geometry of matching in the (R, ρ) coordinates, the calculations in RIOSA are often carried out in planar hyperspherical (PHS) coordinates (q, θ) , $R = q \cos \theta$, $\rho = q \sin \theta$, as well as with simplifying assumptions on the position of matching line, and on relations between the γ 's and angular momenta ℓ in the two spaces [31,38]. To check the quality of RIOSA within a large basis and two-electronic surface system, an extensive series of quantum-mechanical calculations have been recently performed for charge transfer processes in slow collisions of protons with vibrationally excited hydrogen molecules [39]. To include the nuclear rearrangement contribution to the charge transfer process calculations were performed in the PHS coordinates, expanding over large basis sets of vibrational states of both H_2 and H_2^+ , including discretized dissociative continua. This expansion is not uniform in the diatomic vibrational coordinate ρ due to its relation with the hyperradial coordinate q and hyperangle θ , $\rho = q \sin \theta$. This produces nonuniform dissociative continua, which are essential in treating the nuclear rearrangement process. In addition, the Hamiltonian of the problem was modified, following the RIOSA prescription, to include binding potentials of the two nuclear configurations for different ranges of θ , as well as using simplifying assumptions for γ and ℓ relations across the borders [38]. The modified Hamiltonian may have over amplified the promotion dynamics for $\gamma \neq 0$, associated with the saddle in the potential between the two configurations, and thus artificially increased the excitation and dissociation cross sections, suppressing the charge transfer. Finally, the physical boundary conditions for the projectile must be defined along the reactive coordinate R even when using the hyperspherical coordinates. In the limit $R \rightarrow \infty$ (i.e., $q \rightarrow \infty$), the range of θ , which corresponds to the bound vibrational states is small, and thus the asymptotics in q and R lead to the same results uniformly. In practical calculations ($q_\infty = 27$ a.u. in Ref. [39]), the curvature of $\sin \theta$ may significantly influence the results for highly excited initial and/or final vibrational states. Thus, the simplifying RIOSA prescriptions are not fruitful in a large scale calculations.

Some of the previous calculations for $H^+ + H_2$ collisions used the "time dependent" or "impact parameter" formalism that assumes a classical, often straight line, motion of the projectile [16]. While the straight-line trajectory method could be an acceptable approximation for small scattering angles, it poorly describes the scattering at larger angles. Since the scattering angles following vibrational excitation, charge transfer, and nuclear particle exchange for proton impact are shifted significantly toward larger values, a fully quantal approach was chosen here for both the projectile and diatomic vibrational motion in the presence of charge transfer. As in previous work [19,39], the approach of Baer and co-workers [10,11,23,31] is followed with respect to interpretation of IOSA equations and details of transformation from adiabatic to diabatic electronic basis.

III. PRESENT THEORETICAL APPROACH

The problems, originating from RIOSA assumptions as well as from nonuniformity of boundary conditions in PHS coordinates could be partially overcome, at least for a system with a high degree of nuclear symmetry (like H_3^+), by performing the calculation in as large as numerically feasible configuration space of single-nuclear arrangement. Namely, it can be shown that if calculation is done in one nuclear arrangement space exactly it yields the exact transition probabilities, including nuclear arrangements [40]. This is the approach adopted in the present work. Solving for the Schrödinger equation in the large ($R_{\max} = 40$ a.u., $\rho_{\max} = 40$ a.u.) configuration space of initial reactants using very large expansion bases, the transition amplitudes were obtained for charge transfer and excitation, that included also relevant (though inseparable) contributions of nuclear or atomic particle exchange. The drawback of such an approach, inseparability of the nuclear exchange and direct channels, is not essential in applications that involve three equivalent nuclear particles, as is the case here.

In this work the IOSA has been used over the whole energy range considered (0.6–9.5 eV). In principle, caution is needed for a light ion-molecule system since the sudden approximation is expected to be valid for such a system above a collision energy of about 3 eV [15], while for lower energies its validity remains undetermined due to the lack of more elaborate calculations or measurements with which to compare and test it. Nevertheless, since typical rotational energies for H_2 are of the order of 0.01 eV or less, the classical argument of freezing molecular rotations for the duration of the collision for $E > 0.1$ eV indicates that acceptable results may be obtained as long as vibrationally resolved cross sections are calculated. As discussed in Sec. II, the approximate isotropy of the H_3^+ potential surfaces supports this conclusion.

Thus, when the rotational motion of the molecule BC is adiabatic with respect to the relative translational motion of the BC and a colliding particle A , the projectile effectively interacts with a molecule that has no rotational angular momentum. Having in mind that the system evolves under the IOSA constraint $\gamma = \angle(\vec{R}, \vec{\rho}) = \text{const}$, essential for decoupling of all angular momenta of the system, one can expand the wave function in a truncated basis of dimension N of electronic functions $\Phi_n^p(\{\vec{r}_i\}; R, \rho, \gamma)$, $n = 1, 2, \dots, N$, where $\{\vec{r}_i\}$ is the set of electronic coordinates for N_e electrons. Expanding the resulting nuclear functions in partial waves $\psi_n(R, \rho; \gamma, \ell)$ of the angular momentum ℓ of the projectile motion yields two-dimensional Schrödinger equation for nuclear motion in the form of a system of N -coupled partial differential equations of the second order for (uncoupled) partial waves, which can be written in the matrix form and in the mass-scaled coordinates as [39,34,31]

$$[\mathbf{W}^p(R, \rho, \gamma) + (T_N^\ell - E)\mathbf{I}]\Psi(R, \rho; \gamma, \ell) = 0, \quad (5)$$

where Ψ is the state vector with components $\psi_n(R, \rho; \gamma, \ell)$, $n = 1, 2, \dots, N$, \mathbf{I} is the unit matrix, and the kinetic-energy operator takes a simple form

$$T_N^\ell = -\frac{1}{2\mu} \left[\frac{\partial^2}{\partial R^2} + \frac{\partial^2}{\partial \rho^2} - \frac{\ell(\ell+1)}{R^2} \right]. \quad (6)$$

In case of different nuclear arrangements are considered, it is convenient to use the mass-scaled coordinates [41] (R, ρ) obtained from no-scaled coordinates (R', ρ') by the transformation $R = aR', \rho = a^{-1}\rho'$, where $a = (M/m)^{1/4}$, $m = m_B m_C / (m_B + m_C)$ is the reduced mass of the molecule BC , and $M = m_A(m_B + m_C) / (m_A + m_B + m_C)$ is the reduced mass of the $A + BC$ system. The Hamiltonian is then invariant to cyclic permutations of the subscripts A, B , and C (contained in M and m definitions) through all three configurations $k = 1, 2, 3$ of the ABC system [38,31]. Both M and m that would otherwise appear in Eq. (6) are replaced by $\mu = (m_A m_B m_C) / (m_A + m_B + m_C)^{1/2}$, independently of the nuclear configuration, which yields an orthogonal transformation matrix from one arrangement to the other. In case of the H_3^+ system, this feature is not essential, and although it is used here for the generality, the configuration index is omitted in the following.

The potential matrix $\mathbf{W}^p(R, \rho, \gamma)$ depends on a choice p of electronic basis. Thus, for an adiabatic electronic basis $\Phi_n^a(\{\vec{r}_i\}; R, \rho, \gamma)$, with

$$H_{el} \Phi_n^a(\{\vec{r}_i\}; R, \rho, \gamma) = E_n^a(R, \rho, \gamma) \Phi_n^a(\{\vec{r}_i\}; R, \rho, \gamma), \quad (7)$$

where

$$H_{el} = -\frac{1}{2} \sum_{i=1}^{N_e} \nabla_{r_i}^2 + \mathcal{V}(\{\vec{r}_i\}; R, \rho, \gamma), \quad (8)$$

it takes the form $W_{ij}^a(R, \rho, \gamma) = H_{ij} + E_i^a \delta_{ij} = H_{ij}^p + H_{ij}^R + E_i^a \delta_{ij}$, where

$$H_{ij}^x = -\frac{1}{2\mu} \left\{ \sum_{N_i} \left\langle \Phi_i \left| \frac{\partial^2}{\partial x^2} \right| \Phi_j \right\rangle - 2 \sum_{N_i} \left\langle \Phi_i \left| \frac{\partial}{\partial x} \right| \Phi_j \right\rangle \frac{\partial}{\partial x} \right\}, \quad x = \rho, R. \quad (9)$$

The adiabatic electronic basis functions properly describe all distortions experienced by the electronic cloud of a polyatomic system when its geometry is changed very slowly. Generally, the main flaws in this description appear in the calculation and from actual use of matrix elements H_{ij} that arise in the coupled equations. These are particularly poorly behaved near so-called avoided crossing seams and conical intersections of the adiabatic potential-energy surfaces where electronic transitions are most likely to occur. This is the case of the ground and first excited electronic surfaces of the H_3^+ system, with a seam at nearly fixed ρ_s for a wide interval of R . Thus, W_{ij}^a becomes almost a $\delta(\rho - \rho_s)$ function at the seam of H_3^+ , causing numerical breakdown in the calculation, which will be discussed in more detail in Sec. IV.

This difficulty is resolved [31] by transforming to a diabatic basis, here defined by the requirement $H_{ij}^p + H_{ij}^R = 0$, which yields

$$\mathbf{W}^d(E, \rho; \gamma) = \mathbf{A}^T \mathbf{E}^a \mathbf{A}, \quad (10)$$

where $\mathbf{A}(R, \rho; \gamma)$ is the transformation matrix, elaborated in detail by Baer and collaborators [23,31,11], and \mathbf{E}^a is the diagonal matrix of adiabatic energies defined in Eq. (7). Matrix \mathbf{A} satisfies the system of partial differential equations $\partial \mathbf{A} / \partial x + \mathbf{U} \mathbf{A} = 0$, where $x = R, \rho$, and $U_{ij} = \langle \Phi_i | \partial / \partial x | \Phi_j \rangle$. The method of solution was studied in detail for a general case of N electronic surfaces [23]. Obviously, \mathbf{W}^d is a function of integrals of the nonadiabatic matrix elements over both R and ρ , which smooth out any numerically ‘‘violent’’ behavior.

As discussed in Sec. II, the exact Schrödinger equation is invariant to the configuration transformation, and it is irrelevant in which configuration the exact solution is obtained [40] if proper care is taken on boundary conditions. The relevant information which would define the process is contained in the boundary conditions, characteristic of each configuration. The most natural choice for proper definition of the boundary conditions is the initial nuclear arrangement of the reactants, assuming that the configuration space, defined by a two-dimensional box in (R, ρ) plane, is big enough to include other nuclear arrangements of interest.

IV. CALCULATION DETAIL

Significant attention has been paid to obtain reliable electronic adiabatic potential surfaces in the large configuration space of (R, ρ, γ) coordinates. These were constructed, similarly as in Ref. [39], using the diatom-in-molecule (DIM) method [42] to calculate both the lowest adiabatic energy surfaces of H_3^+ and the relevant nonadiabatic electronic matrix elements (of $\partial / \partial R$ and $\partial / \partial \rho$) needed for transformation into the diabatic electronic basis. Although the DIM method might lead to exact potential-energy surfaces (PES) in the limit of a complete basis of excited fragments, the calculation of the H_3^+ DIM surfaces with truncation suggested by Ellison [42] and Preston and Tully [43] is found to be a reasonable accurate, leading to acceptable agreement with the experiment [43,17,11]. This version of the DIM method enables as efficient calculation of the nonadiabatic matrix elements of coupling between various electronic states as of the adiabatic potential-energy surfaces. The matrix elements of nonadiabatic couplings are normally not available from quantum-chemistry calculations.

The suggested truncation involves two lowest gerade and ungerade states, $1s\sigma_g$ and $2p\sigma_u$, of H_2^+ , and the ground state $1\Sigma_g^+$ of the H_2 molecule, resulting in a diagonalization of a 3×3 matrix. $1s\sigma_g$ and $2p\sigma_u$ curves can be calculated with arbitrary accuracy owing to the fact that the one-electron-two-center problem is separable in prolate elliptic coordinates. These curves and their first derivatives were calculated as functions of internuclear distance \mathcal{R} with a step of 0.0002 for $\mathcal{R} \leq 1$ and with a step of 0.001 for $1 < \mathcal{R} \leq 50$ a.u. This enabled a smooth linear fit used for interpolation in the DIM diagonalization. Concerning the H_2 fragment, the best available ground-state singlet potential curve has been used, provided by the extensive compilation of Jamieson [44], slightly modified [45] to remove the discon-

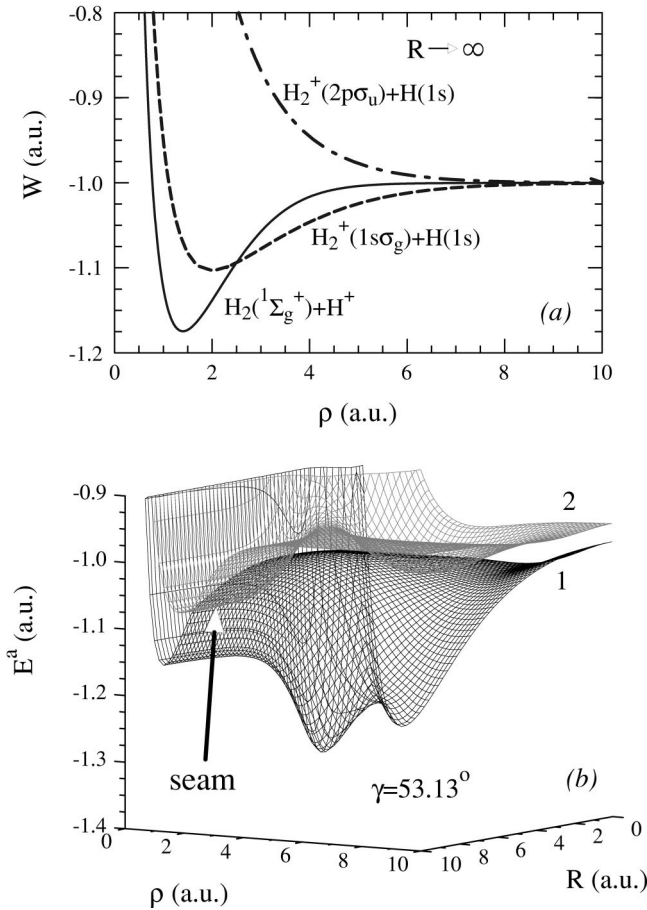


FIG. 1. (a) Diabatic potential curves of the $H_2^+ + H$ and $H + H_2$, at fixed R , for $R \rightarrow \infty$ obtained from three lowest potential curves of H_2 and H_2^+ . (b) The two lowest adiabatic potential surfaces of H_3^+ , at fixed γ .

tinuity present in the derivative of the potential. This contained 678 nonequidistant points between 0.2 and 20 a.u., cubic-spline-fitted in the diagonalization, followed by analytic asymptotic expansion for the long range H_2 potential. Due to numerical feasibility of the DIM, the lowest three-center electronic, adiabatic, potential-energy surfaces (PES) were calculated at more than 10^7 geometries [steps of 0.01 in an interval 0.5–40 for ρ , 0–40 for R , and for six angles γ in interval 0° – 90° (for $\cos \gamma = 0, 0.2, 0.4, 0.6, 0.8$, and 1)]. This enabled a smooth interpolation of the surfaces, especially close to the seam and close to the highly repulsive regions when two nuclei are close, as well as accurate adiabatic-diabatic transformation, good asymptotic potentials, and accurate vibrational energies of the initial and final states.

As mentioned in Sec. III, there is a strong avoided crossing [11,12] between the two lowest PES of the H_3^+ system at $\rho = \rho_s \approx 2.5/a$ a.u., for all $R > \sim a \times 4.5$ a.u., where $a = (4/3)^{1/4}$ is the mass-dependent scaling factor, defined below Eq. (6). Along the seam, $\rho \sim \rho_s$, the matrix elements of $\partial/\partial\rho$ between the adiabatic electronic states become almost δ functions of the vibrational coordinate. This is a consequence of the fact that when $\rho > \rho_s$ for $R \rightarrow \infty$ the $H^+ + H_2$ surface is above the charge transfer surface $H + H_2^+$ [Fig. 1(a)]. In that limit the $H^+ + H_2$ surface becomes a function of

only the diatomic coordinate ρ , i.e., $(H^+ + H_2)(R \rightarrow \infty, \rho, \gamma) \rightarrow H_2(\rho)$. On the other hand, $(H + H_2^+)(R \rightarrow \infty, \rho, \gamma) \rightarrow H(1s) + H_2^+(\rho)$. The two ρ -dependent asymptotic triatomic curves cross at $\rho \approx 2.5/a$ a.u., as can be seen in Fig. 1(a). Thus, if the neutral molecule is in a high enough ($\nu \geq 4$) vibrational state, then on approach of the projectile (H^+ or H) to the (H_2 or H_2^+) target, an almost diabatic transition takes place between the electronic adiabatic surfaces. The third curve is antibonding state $H_2^+(2p\sigma_u) + H(1s)$. The three curves in Fig. 1(a) were used to construct the DIM adiabatic surfaces. The lowest two surfaces, obtained for various angles γ , shown for an example of $\gamma = 53.13^\circ$ in Fig. 1(b), were used as the starting point in present calculations.

To avoid the numerical instabilities due to this triatomic-surface avoided-crossing seam, a transformation for the three lowest H_3^+ adiabatic surfaces into the diabatic representation have been performed, following Baer [10], as explained in Sec. III. The resulting diabatic PES which correspond asymptotically ($R \rightarrow \infty$) to the lowest $H^+ + H_2$ and $H + H_2^+$ in Fig. 1(a) are then chosen for the active electronic surfaces in the calculation. For this transformation one needs nonadiabatic matrix elements between the adiabatic electronic states. These are obtained from the DIM calculation, over the whole configuration space. Figure 2(a) shows the absolute values of nonadiabatic matrix elements of electronic coupling $|U_{12}^\rho| = |\langle 1 | \partial/\partial\rho | 2 \rangle|$, in a part of the configuration space, for an example of $\gamma = 53.13^\circ$. Unlike $U_{12}^R = \langle 1 | \partial/\partial R | 2 \rangle$ (not shown here), U_{12}^ρ has a δ -function-like behavior along the seam.

On the other hand, W_{ij}^d are smooth functions [Fig. 2(b)] in the whole configuration space, much easier to handle numerically. Thus, in the H_3^+ system considered here, a transformation to the diabatic electronic basis is a necessity in the numerical solution of the problem. This is the approach adopted here, and the superscript “ d ” is omitted in the rest of the text. The collision dynamics in the considered energy range evolves at only the two lowest adiabatic (and therefore diabatic) electronic surfaces.

In the case of H_3^+ , one surface corresponds asymptotically to $H^+ + H_2(1\Sigma_g^+)$, and another one to $H(1s) + H_2^+(1s\sigma)$, Fig. 1. In the two-electronic surfaces case, the diabatic potential matrix \mathbf{W} and the state vector Ψ have the forms

$$\mathbf{W} = \begin{bmatrix} W_{11} & W_{12} \\ W_{12} & W_{22} \end{bmatrix}, \quad \Psi = \begin{bmatrix} \Psi_1 \\ \Psi_2 \end{bmatrix}, \quad (11)$$

where the symmetry property of a diabatic matrix is explicitly written. The transformation matrix for this case has a simple form

$$\mathbf{A} = \begin{bmatrix} \cos \alpha & \sin \alpha \\ -\sin \alpha & \cos \alpha \end{bmatrix}, \quad (12)$$

with $\alpha(R, \rho; \gamma) = \alpha(R_0, \rho_0; \gamma) + \int_{\rho_0}^{\rho} U_{12}^\rho(R, \rho; \gamma) d\rho + \int_R^{R_0} U_{12}^R(R, \rho_0; \gamma) dR$. One can assume the complete decou-

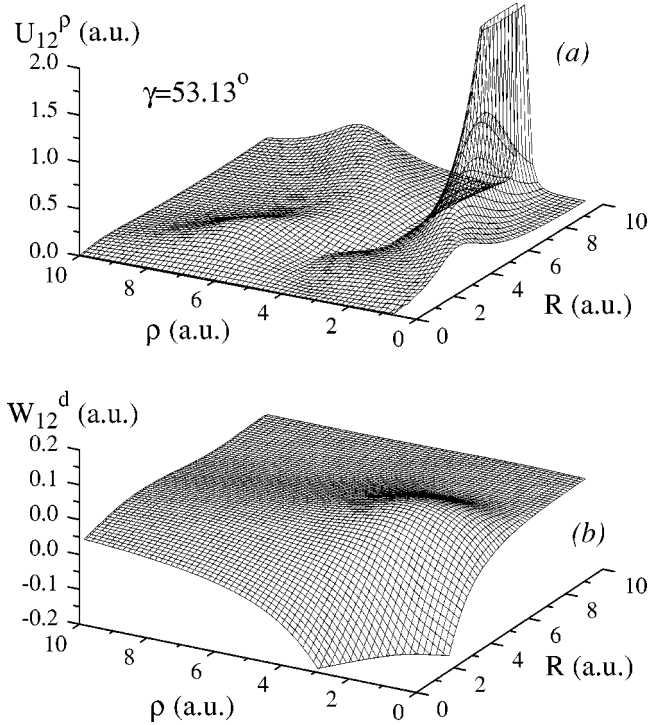


FIG. 2. (a) Surface of nonadiabatic coupling between adiabatic electronic states, $|U_{12}^{\rho}| = |\langle 1 | \partial / \partial \rho | 2 \rangle|$, for a fixed angle γ , and (b) corresponding diabatic coupling.

pling of the adiabatic electronic states for $R_0 = 40$ a.u., $\rho_0 = 0.5$ a.u., i.e., $\alpha(R_0, \rho_0; \gamma) = 0$. The nonadiabatic matrix elements $U_{12}^x = \langle \Phi_1 | \partial / \partial x | \Phi_2 \rangle$, $x = R, \rho$ were obtained from the Feynmann-Hellman theorem [10], using the DIM Hamiltonian and adiabatic eigenstates for the same geometries as the PES (in steps of 0.01, for both R and ρ).

The system of coupled partial differential equations of the second order, Eq. (5), for a chosen configuration (reactant arrangement) can be solved in various ways, depending on the physical parameters of the problem. The usual way is expansion of each component of the vector $\Psi(R, \rho; \gamma)$ in an appropriate complete basis in one of the two variables, R and ρ . For slow collision velocities the expansion in a basis, adiabatic in R , can be a good choice. Thus, in the adiabatic limit of the perturber (projectile) motion, the eigenvalue problem for the coupled vibrational motion on the two diabatic electronic surfaces for each given diatomic orientation angle γ and each fixed value of R , yields an adiabatic basis, parametrically dependent on R, γ . This is obtained by solving the eigenvalue problem for diatomic vibronic motion in the potential W

$$\left[\mathbf{W}(\rho; R, \gamma) - \left(\frac{1}{2\mu} \frac{\partial^2}{\partial \rho^2} + \varepsilon \right) \mathbf{I} \right] \mathbf{V}(\rho; R, \gamma) = 0. \quad (13)$$

This representation reduces the system of partial differential equations, Eq. (5), into a system of ordinary differential equations in R , with nonadiabatic matrix elements of $\partial / \partial R$ and $\partial^2 / \partial R^2$ between the adiabatic vibronic states that follow from Eq. (13). As will be shown elsewhere, the set of vi-

bronic states and corresponding nonadiabatic matrix elements is convenient for qualitative insight into the collision dynamics. Still, this representation is not convenient for numerical solution of the problem. Using the adiabatic basis, emerging from Eq. (13), brings numerical instability into the solution because of “numerically violent” behavior of numerous matrix elements in the zones of narrow avoided crossings between vibronic states. This revives the problems around the seam of the two considered adiabatic electronic surfaces which generated the need to transform adiabatic electronic surfaces into diabatic ones, as discussed in Sec. II.

It is numerically more feasible to use a diabatic vibrational basis, obtained for a single, fixed value of R in Eq. (13). The usual choice $R \rightarrow \infty$ yields the diagonal matrix for $\mathbf{W}(\rho; R \rightarrow \infty, \gamma)$, and the eigenvalue problem (13) is reduced to a set of uncoupled eigenvalue problems for vibrational motion on each diabatic electronic surface. The resulting basis $\{u_k^{(n)}(\rho)\}$ for each $\Psi_n(R, \rho, \gamma)$ in Eq. (11) is a vibrational basis for the isolated diatomic molecule (H_2 for $n=1$ and H_2^+ for $n=2$) in a corresponding electronic state. Thus, expanding

$$\Psi_i(R, \rho, \gamma) = \sum_k f_k^{(i)}(R, \gamma) u_k^{(i)}(\rho), \quad (14)$$

Eq. (5) takes the form

$$\left\{ \mathbf{D}(R) - \left[\frac{1}{2\mu} \left(\frac{\partial^2}{\partial R^2} \right) + E - \frac{\ell(\ell+1)}{2\mu R^2} - \varepsilon(R; \gamma) \right] \mathbf{I} \right\} \mathbf{F}(R, \gamma) = 0, \quad (15)$$

where

$$\mathbf{D} = \begin{bmatrix} \mathbf{D}^{11} & \mathbf{D}^{12} \\ \mathbf{D}^{12} & \mathbf{D}^{22} \end{bmatrix}, \quad \mathbf{F} = \begin{bmatrix} \mathbf{F}^{(1)} \\ \mathbf{F}^{(2)} \end{bmatrix}, \quad \varepsilon = \begin{bmatrix} \varepsilon^{(1)} & 0 \\ 0 & \varepsilon^{(2)} \end{bmatrix}, \quad (16)$$

$$D_{nm}^{IJ}(R; \gamma) = \int d\rho u_n^I(\rho) [W_{IJ}(\rho; R, \gamma) - \delta_{IJ} \mathbf{W}_{IJ}(\rho; R \rightarrow \infty, \gamma)] u_m^J(\rho). \quad (17)$$

The components of the subvectors $\mathbf{F}^{(I)}(R, \gamma)$ and diagonal matrix $\varepsilon^{(I)}$ are the amplitudes and energies, respectively, of vibrational states belonging to an electronic state I , where $I = 1, 2$ correspond to the ground states of H_2 and H_2^+ , respectively. The matrix elements of the matrix \mathbf{D} were done by numerical integration, for all combinations (m, n) of vibrational functions within the chosen basis. When $R \gg \rho$ the potential matrix $\mathbf{W}(\rho; R \rightarrow \infty, \gamma)$ is independent of γ .

Thus, the diabatic vibronic expansion bases for $\Psi_{1,2}$ are truncated sets of vibrational states of H_2 and H_2^+ in ground electronic states. The eigenvalue problem (13), with $R \rightarrow \infty$, was solved with finite quantization “volume” boundary conditions, $u_k^{(n)}(\rho_{\max}) = u_k^{(n)}(\rho = 0.5) = 0$, where $\rho_{\max} = 40$ a.u., discretizing the interval (0.5, 40) a.u. along the ρ axis in 450 mesh points. This resulted in 450 vibrational states on each of H_2 and H_2^+ , of which 34 are bound and 866 are continuum pseudostates. Although the relevant vibronic continua

are discretized, with this large ρ_{\max} the density of the continuum states (largest close to the continuum edge) stays high even for several eV above the continuum edge. The discretization of the dissociative continuum was used earlier by Onda [47] to calculate the dissociation of H_2 by H impact, but with a much smaller number of states.

To solve the system of coupled-second-order ordinary differential equations in amplitudes \mathbf{F} , proper plane-wave boundary conditions have to be applied at entrance exit of the reactant configuration, i.e., at $R=R_{\max}=40$ a.u. An efficient and accurate numerical procedure was employed utilizing multichannel logarithmic derivatives. It is convenient to introduce the \mathbf{K} matrix for each ℓ [46],

$$\Psi(R>R_{\max})=\mathbf{J}(R)+\mathbf{N}(R)\mathbf{K}, \quad (18)$$

where the elements of the diagonal matrices $\mathbf{J}(R)$ and $\mathbf{N}(R)$ are composed of the Riccati-Bessel functions of the first and second kind for open channels, and of modified spherical Bessel functions of the first and the third kind for closed channels. The \mathbf{K} matrix is an augmented reaction matrix containing elements connecting closed as well as open channels, i.e., \mathbf{K} can be written in the form

$$\mathbf{K}=\begin{pmatrix} \mathbf{K}_{oo} & \mathbf{K}_{oc} \\ \mathbf{K}_{co} & \mathbf{K}_{cc} \end{pmatrix}, \quad (19)$$

where oo , oc , co , and cc are indices for open-open, open-close, close-open and close-close submatrices of \mathbf{K} . The \mathbf{S} matrix is then given in terms of the open-open submatrix, i.e.,

$$\mathbf{S}=(1+i\mathbf{K}_{oo})^{-1}(1-i\mathbf{K}_{oo}). \quad (20)$$

The index ℓ has been omitted from Eqs. (18)–(20). In the case of explicit treatment of the nuclear particle exchange the \mathbf{K} and \mathbf{S} matrices can be further augmented with the submatrices for transitions within and between various nuclear configurations, still keeping the same formalism as above, applying appropriate boundary conditions for each configuration.

Since, during a collision with particle A , various, instantaneous directions of the molecule BC are equally possible, the cross section must be averaged over the full solid angle of BC orientations, which leads to averaging over γ . The problem must be solved for various γ in order to permit such an averaging. In nuclear-symmetric systems, such as H_3^+ , symmetry around $\gamma=90^\circ$ reduces necessary calculations to $0^\circ \leq \gamma \leq 90^\circ$, rather than to $0^\circ \leq \gamma \leq 180^\circ$, as is the case generally. The differential cross section for transition from a state ν in the manifold of vibrational states of the electronic state n to a state (n', ν') is then obtained, within IOSA, in the form

$$\frac{d\sigma_{n\nu, n'\nu'}(\theta)}{d\Omega} = \frac{1}{8k_{nj}^2} \int_0^\pi d\gamma \sin \gamma \left| \sum_{\ell} (2\ell+1) P_{\ell}(\cos \theta) \times [\delta_{nn'} \delta_{\nu\nu'} - S_{n\nu, n'\nu'}^{\ell}(\gamma)] \right|^2, \quad (21)$$

where θ is the scattering angle, and accordingly, the integral cross section follows as

$$\sigma_{n\nu, n'\nu'} = \frac{\pi}{2k_{nj}^2} \int_0^\pi d\gamma \sin \gamma \sum_{\ell} (2\ell+1) |\delta_{nn'} \delta_{\nu\nu'} - S_{n\nu, n'\nu'}^{\ell}(\gamma)|^2. \quad (22)$$

This simple result expresses the vibronic cross sections as an average over γ of the relevant differential, $d\sigma_{n\nu, n'\nu'}(\theta, \gamma)/d\Omega$, and integral, $\sigma_{n\nu, n'\nu'}(\gamma)$, cross sections.

It was unnecessary to use the whole basis set of 900 states. At the lowest energies of the considered range ($E_{c.m.}=0.6$ eV), the necessary number of states to achieve convergence of the charge transfer cross sections for $\text{H}+\text{H}_2^+$ system was $N=205$. Similarly, more than hundred states was needed for convergence of the excitation cross section into the first excited state of H_2 by proton impact although only two states, the ground and the first excited state of H_2 belong to the open-channel manifold. For the highest energies, $E_{c.m.}=9.5$ eV, convergence of CT for the H^++H_2 system was achieved by $N=560$ states. The needed large number of basis states of ‘‘closed channels’’ stresses the importance of transitions in the strongly deformed small- R region, in particular, with nuclear particle exchange.

Since the wavelength of the free proton motion varies approximately between 0.75 and 0.18 a.u. for a kinetic-energy interval between 0.5 and 9.5 eV, it could be expected that a step ΔR of R not much less than 0.01 a.u. would be small enough to reach convergence in a numerical solution for the integral cross sections. A three-digit convergence for representative cross sections was reached with $\Delta R=0.01$ at $E_{c.m.}=5$ eV, but with $\Delta R=0.001$ for $E_{c.m.}=9.5$ eV. Following this investigation, the calculation was done with $\Delta R=0.01$ for energies 0.6–5 eV, while for higher energies $\Delta R=0.001$ was used.

A convergence check in number of partial waves ℓ_{\max} was accomplished by considering the sum of transition probabilities to all inelastic channels. Thus, ℓ_{\max} was defined for each diatomic-orientation angle γ as the value of ℓ when the sum reached a stable value of 10^{-4} (for 20 partial waves in succession). A weak dependence of ℓ_{\max} on the molecular orientation (γ) was observed.

The full \mathbf{S} matrices were calculated with the collision energy defined in range (0.6,9.5) eV of the triatomic center-of-mass system, with reference to the ground vibrational state of H_2 . The transitions from the excited states were then obtained by an appropriate shift of the reference energy.

V. CHARGE TRANSFER AND EXCITATION RESULTS

The total transition cross section from a vibrational state ν_i of the target molecule (H_2 or H_2^+), $\sigma_T(\nu_i)$, is defined as the sum over all final states ν_f of the partial cross sections for transition from ν_i to a ν_f , i.e., $\sigma_T(\nu_i)=\sum_{\nu_f} \sigma_T(\nu_i \rightarrow \nu_f)$. Depending on the process (charge transfer or excitation) ν_f may belong to H_2^+ or H_2 .

Figure 3 shows the total charge transfer $\sigma_{CT}(\nu_i)$ cross

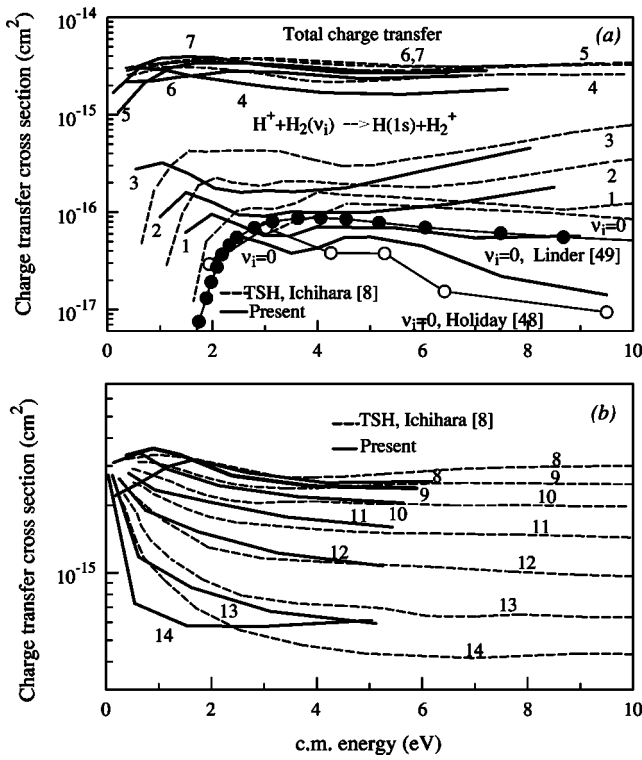


FIG. 3. Total integral cross section for charge transfer from various initially excited vibrational states ν_i for $H^+ + H_2(\nu_i) \rightarrow H + H_2^+$ collisions (thick solid lines); filled symbols, the data for $\nu_i=0$ recommended by Linder *et al.* [49]; hollow symbols, experimental results of Holiday [48]; dashed lines, TSH calculation of Ichihara *et al.* [8].

section for the reaction in Eq. (1), as a function of energy for the initial ground $\nu_i=0$, and 14 ($\nu_i=1, 2, \dots, 14$) excited states of H_2 . Comparisons with the experimental results of Holiday *et al.* [48], and the recommended data of Linder [49] for $\nu_i=0$ are also shown. Typical results of the TSH calculations of Ichihara *et al.* [8] are displayed as well. While at collision energies $E_{c.m.} < 5$ eV our result agrees very well with the data of Holiday, deviation between the two sets reaches 50% at 6.5 eV, but decreases to 10% at about 9 eV. While our curve overestimates the Holiday data at a few eV c.m. energy, it underestimates the Linder recommended data (based on another experiment [49] for the same process). Thus, experimental data of Linder and Holiday deviate mutually by a factor of 2 at energies above 6 eV, which can be associated to experimental difficulties in control of the initial vibrational state content of the H_2 target. Our curve for $\nu_i=0$ almost averages the two sets of the experimental reference data. The increasing agreement of the TSH results with increase of ν_i and energy is expected from the classical character of the TSH model. Absence in TSH results of the inversion, seen in our quantal calculations for the $\nu_i=13$ and $\nu_i=14$ curves at $E_{c.m.} \sim 5$ eV, can be most likely attributed to the small differences in the two calculations of the vibrational configuration spaces for larger ρ . It is interesting to note that the TSH calculations [8] obtain the contributions due to nuclear particle exchange separately, and their curves in Fig. 3 are sums of the “direct” and particle exchange CT.

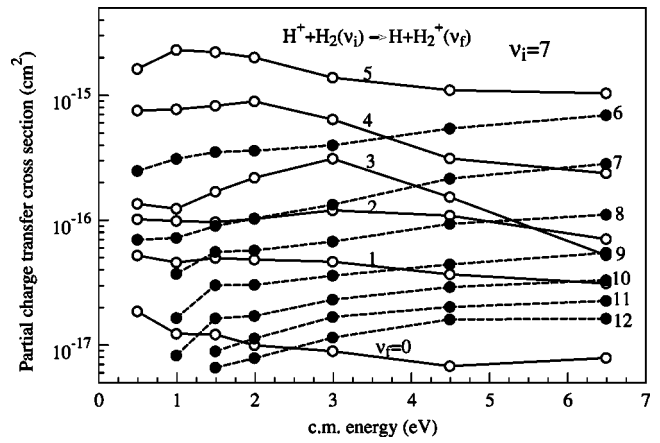


FIG. 4. Final state resolved charge transfer cross section for $H^+ + H_2(\nu_i=7)$.

The latter peaks at smallest energies where it becomes the dominant contribution, especially for higher ν_i . Our calculation, which implicitly takes nuclear exchange into account, shows good agreement with these total TSH curves in the classical range of validity.

The final-state resolved partial cross sections for CT in $H^+ + H_2(\nu_i)$ collisions, are shown in Fig. 4 as functions of the collision energy for a representative value of $\nu_i=7$, and for ν_f of H_2^+ less than 12. This is an exoergic process and the partial cross sections are largest between the states closest in vibrational energy $W(\nu_f) < W(\nu_i)$. Figure 5 shows the distribution of the partial cross section for CT over the final vibrational states H_2^+ , for several representative values of collision energy and for (a) $\nu_i=13$, and (b) $\nu_i=4$. The overlapping features of the curves for various energies lead to a weak dependence of the total CT cross section on energy, as seen in Fig. 3. The apparent peak for CT from $\nu_i=4$ into the lowest states of H_2^+ reflects a quaresonance of $\nu_i=4$ at H_2 and $\nu_f=0$ at H_2^+ , where $W(\nu_i=4) > W(\nu_f=0)$.

Integral cross sections for charge transfer processes in the $H + H_2^+$ collision system are shown in Figs. 6. For comparison, CT from $H_2^+(\nu_i=0)$ is repeated in Figs. 6(b), 6(c), and 6(d). As can be seen, the spread of the cross sections for CT from different initial states, $H_2^+(\nu_i)$, is much smaller than in case of the charge transfer from the H_2 target, reflecting the exoergic nature of the former process. Excluding the highest states in the vibrational manifold of H_2^+ , which are rapidly depleted to the dissociative continuum, all CT cross sections for various ν_i lie within half of an order of magnitude in the considered range of collision energies. The oscillations in the cross section with energy, studied earlier in experiment [50] and in theory [50–52] of charge transfer and excitations in slow ion-atom collisions, can also be seen in Figs. 6(a), 6(b), and 6(c). These might be a consequence of interference of various channels of similar transition intensity, leading to the total cross section for charge transfer, as well as of competition of the charge transfer and vibrational excitation-deexcitation channels. The channels are characterized by both different transition mechanisms, at different distance R , as well as by multiplicity of vibrational states that take part in charge transfer from an initial vibrational state.

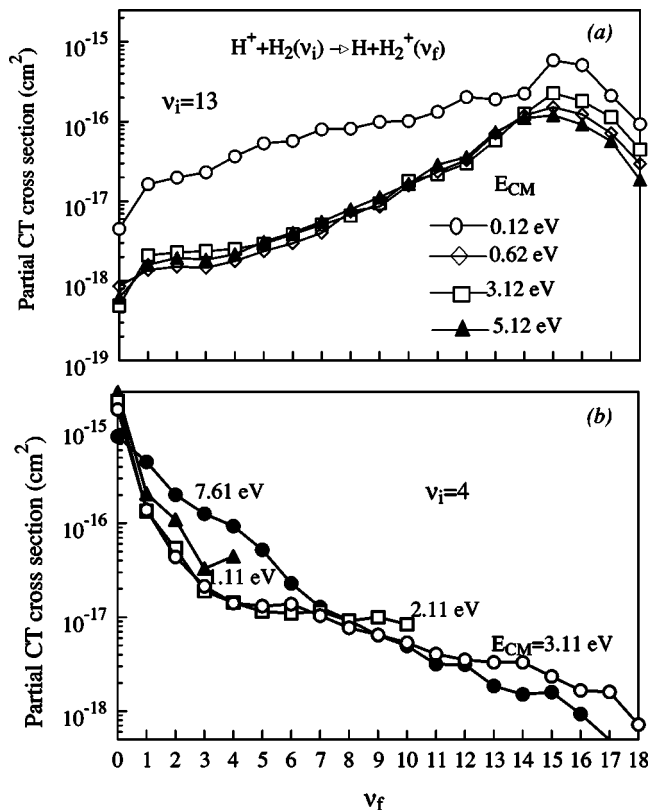


FIG. 5. Distribution of the CT cross section over final vibrational states ν_f of H_2^+ for representative values of the c.m. collision energy $E_{c.m.}$ from (a) $H_2(\nu_i=4)$ and (b) $H_2(\nu_i=13)$.

The partial, final state resolved CT cross sections for $H+H_2^+(\nu_i=0)$ reaction are shown in Fig. 7. Due to the quasiresonances with $\nu_f=0$ of H_2 , charge transfer is overwhelmingly dominated by the transition to $\nu_f=4$.

Figure 8 shows the distribution of the partial CT cross section over the final states in ν_f of H_2 from $\nu_i=13$ of H_2^+ , for representative values of the collision energy. Obviously in this case, the CT is dominated by the transitions to almost resonant states of the final molecule, nearly independently of energy. It is interesting to note that for lower ν_f the partial

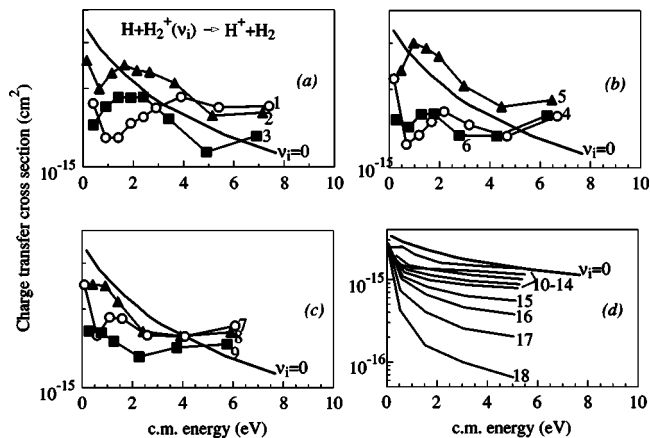


FIG. 6. Total integral cross section for charge transfer from $H(1s)$ to the $H_2^+(\nu_i)$ target.

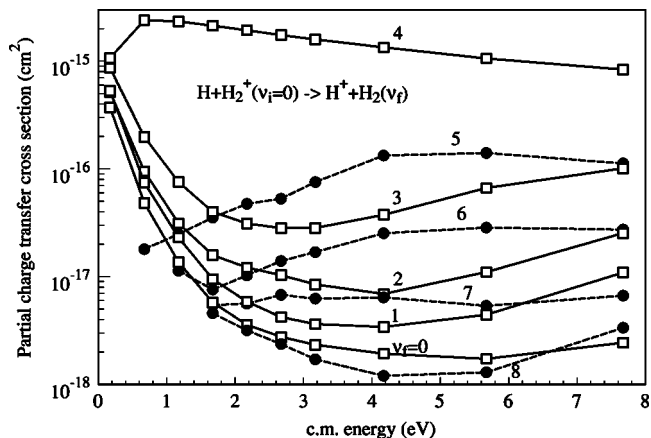


FIG. 7. Final state ν_f resolved CT cross section for $H(1s) + H_2^+(\nu_i=0) \rightarrow H^+ + H_2(\nu_f)$ process.

CT cross sections are significantly larger at lower energies, in agreement with the behavior of the integral cross section for $\nu_i=13$ in Fig. 6(d).

The results for vibrational excitation are presented in Figs. 9–12. Thus, Fig. 9 shows the partial excitation cross sections from the vibrational ground state of H_2 in collisions with protons, Eq. (3). Previous quantal calculations of Schinke *et al.* [16,15] and Giese and Gertry [13] were done only with an incomplete set of bound vibrational states, in a small configuration space, thus not taking into account nuclear particle exchange into excited vibrational states. As a consequence, their results persistently underestimate the excitation cross sections at lowest energies. After the threshold, the excitation cross sections from $\nu_i=0$ to a final state ν_f first rise steeply [19] to their respective values, and then continue to rise much more slowly until opening of the next excitation channel (ν_f+1), after which it drops. This trend of decrease with opening of a new excitation channel, as well as of charge transfer channels (about 2 eV of c.m. energy), can be seen for lower states (below the charge transfer threshold) until the dissociation threshold (about 4.5 eV) is

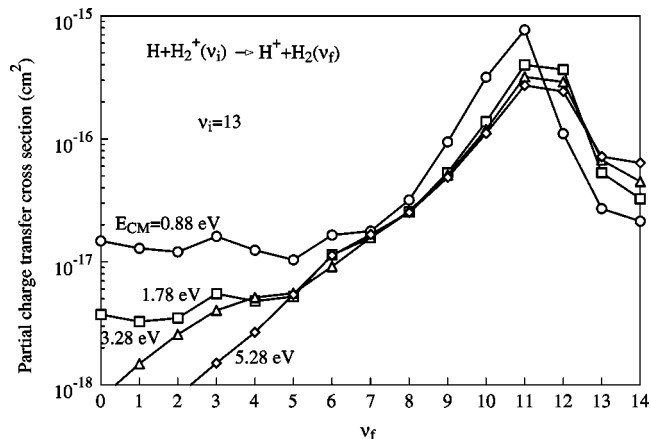


FIG. 8. Distribution of the partial CT cross sections over the final vibrational states ν_f of H_2 for the process $H(1s) + H_2^+(\nu_i=13) \rightarrow H^+ + H_2(\nu_f)$.

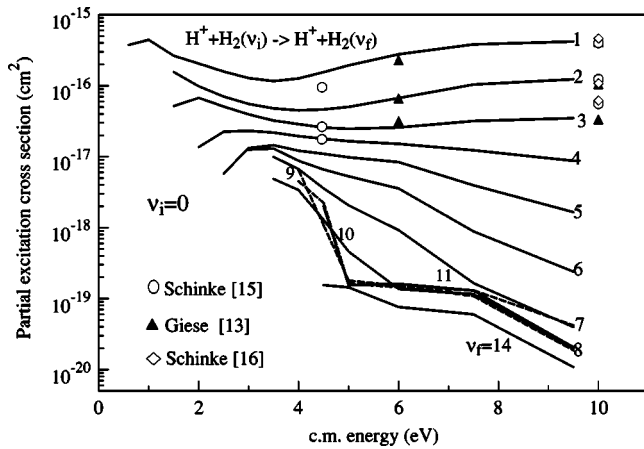


FIG. 9. Vibrational excitation from the ground state $v_i=0$ to the final state v_f of H_2 in collision with proton. Solid lines are the present results; circles are the calculation of Schinke *et al.* [15], triangles the calculation of Giese *et al.* [13], diamonds the calculation of Schinke [16].

reached. On the other hand, the final states $v_f \geq 4$ are partially depleted by charge transfer, resulting in the steady decrease of the excitation cross section with energy, after an initial jump at the threshold. Fig. 10 shows the excitation cross section of H_2^+ , initially in the ground vibrational state, into all v_f of H_2^+ . It shows features of the cross section with energy similar to Fig. 9, except that these are smoothed by 1) the increased density of the vibrational states in the shallow H_2^+ potential well in comparison to the step in energy (0.5–1 eV) used in calculation, (2) exoergic nature of the CT channels, and (3) closeness of the dissociation threshold (about 2.5 eV).

Figures 11 and 12 show the total excitation cross sections, summed over final states, for each of the two systems, $H^+ + H_2(v_i)$ (Fig. 11) and $H + H_2^+(v_i)$ (Fig. 12), for various representative initial states v_i . Summations were done for all opened channels $v_f \neq v_i$, irrespectively whether v_f corresponds to excitation or deexcitation. For the case in Fig. 11 the recommended cross section exists by Janev *et al.* [53] for

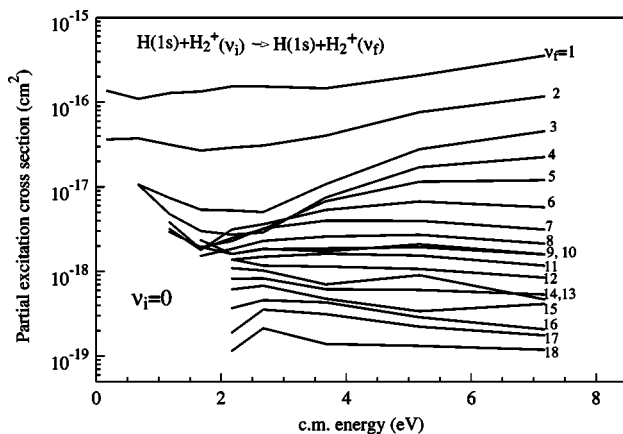


FIG. 10. Vibrational excitation from the ground state, $v_i=0$, to the final state v_f of H_2^+ in collision with H.

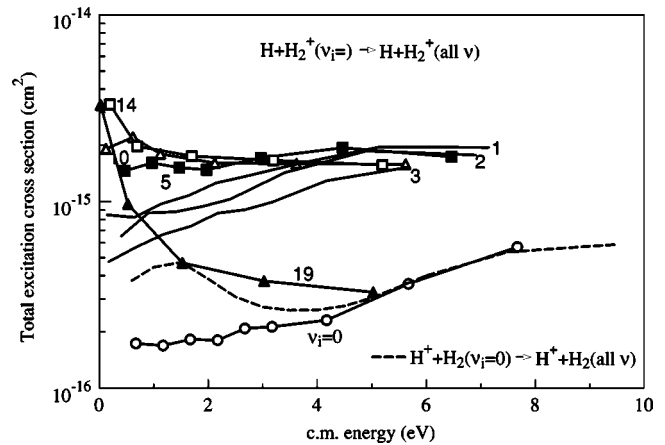


FIG. 12. Vibrational excitation-deexcitation of H_2^+ in collision with H from an initial state v_i , summed over final states v_f .

$v_i=0$ and for sum over $v_f < 5$. There is an increasing disagreement of the recommended and our $v_i=0$ curves with decreasing collision energy, which cannot be explained by a role of the final states $v_f \geq 5$ (Fig. 11). The agreement is acceptable at the higher end of the considered energy range.

It is interesting to note that excitation and charge transfer cross sections are very similar in magnitude. Even in the case of $H^+ + H_2$ system, excitation to higher than $v_f=4$ states is of the same order of magnitude as the relevant charge transfer cross sections. This strongly stresses the need to calculate all inelastic cross sections on the “same footing.”

The tables of all initial- and final-state resolved, as well as the total cross sections for charge transfer and excitation in collision systems $H^+ + H_2(v_i)$ and $H + H_2^+(v_i)$ are available at the web site (www-cfadc.phy.ornl.gov).

VI. CONCLUSIONS

A comprehensive quantum-mechanical study of inelastic processes between bound vibrational states on the coupled

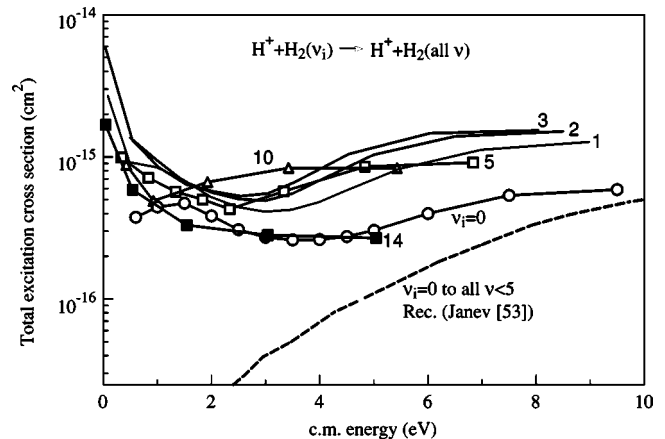


FIG. 11. Vibrational excitation-deexcitation of H_2 in collision with protons from an initial state v_i , summed over final states v_f ; dashed line is the recommended curve from literature [53] for $v_f \leq 4$.

ground electronic surfaces, $H^+ + H_2$ and $H + H_2^+$, of the H_3^+ collision system has been performed. Both charge exchange and excitation from $H_2(\nu_i)$ in collision with protons and from $H_2^+(\nu_i)$ in collision with hydrogen atoms, for all excited initial vibrational states ν_i were computed in the presence of the relevant coupled, discretized vibrational continua, and in the large configuration spaces of the reactants, to account for the transitions through the “closed” channels, in particular, for the transitions through the dissociative continuum as well as with the nuclear particle exchange involved. Results obtained for total and final-state resolved cross sections were reported in the range of 0.6–9.5 eV center-of-mass collision energies. The main approximation used was IOSA which implies the freezing of the target molecule rotations during the collision, and post collisional av-

eraging over the molecule orientations. Choice of this approximation set the lower limit of the considered range of collision energies to a fraction of eV. Comparisons were done with previous quantal and TSH calculations. These confirm applicability of the classical prescriptions of TSH for the total cross sections at energies above 10 eV, as well as for transitions among highly excited vibrational states.

ACKNOWLEDGMENTS

I acknowledge support from the U.S. Department of Energy, Office of Fusion Energy Sciences, through Oak Ridge National Laboratory, managed by UT-Battelle, LLC, under Contract No. DE-AC05-00OR22725.

-
- [1] S. I. Krasheninnikov, A. Yu. Pigarov, and D. J. Sigmar, *Phys. Lett. A* **214**, 285 (1996).
- [2] A. Yu. Pigarov and S. I. Krasheninnikov, *Phys. Lett. A* **222**, 251 (1996).
- [3] S. I. Krasheninnikov, A. Yu. Pigarov, T. K. Soboleva, and D. J. Sigmar, *J. Nucl. Mater.* **241-243**, 283 (1997).
- [4] S. I. Krasheninnikov, A. Yu. Pigarov, D. A. Knoll, B. LaBombard, B. Lipschultz, D. J. Sigmar, T. K. Soboleva, J. L. Terry, and F. Wising, *Phys. Plasmas* **4**, 1638 (1997).
- [5] R. K. Janev, *Contrib. Plasma Phys.* **38**, 307 (1998).
- [6] P. C. Stancil, S. Lepp, and A. Dalgarno, *Astrophys. J.* **509**, 110 (1998).
- [7] A. V. Phelps, *J. Phys. Chem. Ref. Data* **19**, 653 (1990).
- [8] A. Ichihara, O. Iwamoto, R. K. Janev, *J. Phys. B* **33**, 4747 (2000).
- [9] J. C. Tully and R. K. Preston, *J. Chem. Phys.* **55**, 562 (1971).
- [10] M. Baer, G. Niedner, and J. P. Toennies, *J. Chem. Phys.* **88**, 1461 (1988).
- [11] M. Baer, G. Niedner-Schatteburg, and J. P. Toennies, *J. Chem. Phys.* **91**, 4169 (1989).
- [12] A. Ichihara and K. Yokoyama, *J. Chem. Phys.* **103**, 2109 (1995).
- [13] C. F. Giese and W. R. Gentry, *Phys. Rev. A* **10**, 2156 (1974).
- [14] R. Schinke, M. Dupuis, and A. Jr. Lester, *J. Chem. Phys.* **72**, 3909 (1980), and references therein.
- [15] R. Schinke and P. McGuire, *Chem. Phys.* **31**, 391 (1978).
- [16] R. Schinke, *Chem. Phys.* **24**, 379 (1977).
- [17] G. Neidner, M. Noll, J. P. Toennies, and Ch. Schlier, *J. Chem. Phys.* **87**, 2685 (1987).
- [18] M. Kimura, *Phys. Rev. A* **32**, 802 (1985).
- [19] P. S. Krstić and D. R. Schultz, *J. Phys. B* **32**, 2415 (1999).
- [20] P. S. Krstić and D. R. Schultz, *At. Plasma-Mater. Interac. Data Fusion* **8**, 1 (1999).
- [21] P. S. Krstić and D. R. Schultz, in *Atomic Processes in Plasmas* edited by R. C. Mancini and R. A. Phaneuf, AIP Conf. Proc. No. 547 (AIP, Melville, NY, 2000), p. 53.
- [22] Z. H. Top and M. Baer, *Chem. Phys. Lett.* **39**, 134 (1976).
- [23] Z. H. Top and M. Baer, *J. Chem. Phys.* **66**, 1363 (1977).
- [24] Z. H. Top and M. Baer, *Chem. Phys.* **25**, 1 (1977).
- [25] D. Secrest, *J. Chem. Phys.* **62**, 710 (1975).
- [26] R. T. Pack, *J. Chem. Phys.* **60**, 633 (1974).
- [27] S. I. Chu and A. Dalgarno, *Proc. R. Soc. London, Ser. A* **342**, 191 (1975).
- [28] V. Khare, *J. Chem. Phys.* **68**, 4631 (1978).
- [29] D. J. Kouri, in *Atom Molecule Collision Theory*, edited by R.B. Bernstein (Plenum Press, New York, 1979).
- [30] *Theory of Chemical Reaction Dynamics*, edited by M. Baer (CRC Press, Boca Raton, FL, 1985), Vols. I and II.
- [31] M. Baer and H. Nakamura, *J. Chem. Phys.* **87**, 4651 (1987).
- [32] A. Kupperman, G. Schatz, and M. Baer, *J. Chem. Phys.* **65**, 4596 (1976).
- [33] G. C. Schatz and A. Kupperman, *J. Chem. Phys.* **65**, 4642 (1976).
- [34] V. Sidis, *Adv. At. Mol. Phys.* **25**, 161 (1989).
- [35] V. Khare, D. J. Kouri, and M. Baer, *J. Chem. Phys.* **71**, 1188 (1979).
- [36] J. M. Bowman and K. Tung Lee, *J. Chem. Phys.* **72**, 5071 (1980).
- [37] M. Baer, D. J. Kouri, and J. Jellinek, *J. Chem. Phys.* **80**, 1431 (1984).
- [38] H. Nakamura, A. Ohsaki, and M. Baer, *J. Phys. Chem.* **90**, 6176 (1986).
- [39] P. S. Krstić, D. R. Schultz, and R. K. Janev, **T96**, 61 (2002).
- [40] K. T. Tang, in *Theory of Chemical Reaction Dynamics II*, edited by M. Baer (CRC Press, Boca Raton, FL, 1985).
- [41] L. M. Delves, *Nucl. Phys.* **20**, 275 (1960).
- [42] F. O. Ellison, *J. Am. Chem. Soc.* **85**, 3540 (1963).
- [43] R. K. Preston and J. K. C. Tully, *J. Chem. Phys.* **54**, 4297 (1971).
- [44] M. J. Jamieson, A. Dalgarno, and J. N. Yukich, *Phys. Rev. A* **46**, 6956 (1992).
- [45] D.R. Schultz, S.Yu. Ovchinnikov, and S.V. Passovets, in *Atomic and Molecular Processes in Fusion Edge Plasmas*, edited by R.K. Janev (Plenum, New York, 1995), p. 279.
- [46] B. Johnson, *J. Comput. Phys.* **13**, 445 (1973).
- [47] K. Onda, *J. Phys. B* **24**, 4509 (1991).
- [48] M. G. Holliday, J. T. Muckerman, and L. Friedman, *J. Chem. Phys.* **54**, 1058 (1971).
- [49] F. Linder, R. K. Janev, and J. Botero, in *Atomic and Molecular Processes in Fusion Edge Plasmas* (Ref. [45]), p. 397.

- [50] J. S. Thompson, A. M. Covington, P. S. Krstić, M. Pieksma, J. L. Shimpagh, P. C. Stancil, and C. C. Havener, *Phys. Rev. A* **63**, 012717 (2001).
- [51] D. R. Schultz, C.O. Reinhold, and P.S. Krstić, *Phys. Rev. Lett.* **78**, 2720 (1997).
- [52] P. S. Krstić, C. O. Reinhold, and D. R. Schultz, *J. Phys. B* **31**, L155 (1998).
- [53] R. K. Janev, W. D. Langer, K. Evans, Jr, and D. E. Post, Jr., in *Elementary Processes in Hydrogen-Helium Plasmas* (Springer-Verlag, New York, 1987).